Laser and Particle Beams (2013), *31*, 379–386.

doi:10.1017/S0263034613000359

Generation of hemispherical fast electron waves in the presence of preplasma in ultraintense laser-matter interaction

X. H. YANG,[1] Y. Y. MA,[1,*] H. XU,[2] F. Q. SHAO,[1] M.Y. YU,[3,4] Y. YIN,[1] H. B. ZHUO,[1] AND M. BORGHESI[5,6]

[1]College of Science, National University of Defense Technology, Changsha, China
[2]State Key Lab of High Performance Computing, School of Computer Science, National University of Defense Technology, Changsha, China
[3]Institute for Fusion Theory and Simulation, Zhejiang University, Hangzhou, China
[4]Institut für Theoretische Physik I, Ruhr-Universität Bochum, Bochum, Germany
[5]Centre for Plasma Physics, School of Mathematics and Physics, Queen's University of Belfast, Belfast, United Kingdom
[6]Institute of Physics of the ASCR, ELI-Beamlines project, Prague, Czech Republic

(Received 19 February 2013; Accepted 26 March 2013)

Abstract

Hemispherical electron plasma waves generated from ultraintense laser interacting with a solid target having a subcritical preplasma is studied using particle-in-cell simulation. As the laser pulse propagates inside the preplasma, it becomes self-focused due to the response of the plasma electrons to the ponderomotive force. The electrons are mainly heated via betatron resonance absorption and their thermal energy can become higher than the ponderomotive energy. The hot electrons easily penetrate through the thin solid target and appear behind it as periodic hemispherical shell-like layers separated by the laser wavelength.

Keywords: Betatron resonance; Electron plasma waves; Ponderomotive force; Preplasma

INTRODUCTION

Fast electrons generation in ultraintense laser-solid interaction have been investigated extensively both theoretically and experimentally (Sentoku *et al.*, 2006; Kemp *et al.*, 2009; Nilson *et al.*, 2011) because of their application in laser-plasma accelerators (Borghesi *et al.*, 2006; Yu *et al.*, 2009; Yang *et al.*, 2010), fast ignition (FI) schemes of inertial confinement fusion (Tabak *et al.*, 1994; Deutsch & Didelez, 2011), bright X-ray sources (Pfeifer *et al.*, 2006), etc. The energy spectrum, spatial distribution, and divergence angle of the energetic electrons can be significantly affected by the ubiquitous low-density blow-off plasma (the preplasma) created by the inherent laser prepulse and/or spontaneous emissions from the lasing system (Nuter *et al.*, 2008; Davies *et al.*, 2009; MacPhee *et al.*, 2010; Cai *et al.*, 2010; Lin *et al.*, 2012; Sakagami *et al.*, 2012). Thus, the effect of the preplasma should be taken into account in studies of fast electron generation from intense laser-solid target interaction.

Interaction of an intense laser pulse with a solid target having a large preplasma can involve nonlinear processes such as self-focusing, filamentation, hole-boring, etc. that can play important roles in the generation and propagation of fast electrons (Pukhov & Meyer-ter-Vehn *et al.*, 1996; Friou *et al.*, 2012). Fast electrons are also generated in the preplasma, and it has been found that they usually have a two-temperature Maxwellian distribution. The temperature of the high-energy component is much higher than the ponderomotive energy (Wilks *et al.*, 1992) and it scales with the length L_p of the preplasma. The heating can be attributed to betatron resonance absorption (Pukhov *et al.*, 1999; Gahn *et al.*, 2000), Laser Wake Field Acceleration (LWFA) (Tajima *et al.*, 1979), stochastic heating (Sheng *et al.*, 2002; Paradkar *et al.*, 2010), etc. The efficiency of laser-to-electron energy conversion should thus increase with L_p. However, Ma *et al.* (2012) recently found that it can actually decrease for fast (1–3 MeV, corresponding to the optimum energy for FI) electrons. Moreover, the spatial divergence of the fast electrons also increases with L_p. Thus, in order to realize FI it is necessary to manage the prepulse.

The quasistatic electric and magnetic fields produced spontaneously in the preplasma during the laser-plasma interaction can also affect the fast electron generation and transport (Wei *et al.*, 2008; Kemp *et al.*, 2010). The spontaneous magnetic fields can in turn be enhanced locally by

*Address correspondence and reprint requests to: Y. Y. Ma, College of Science, National University of Defense Technology, Changsha 410073, China. E-mail: plasim@163.com

the onset of Weibel-like instabilities, which together with the relativistic displacement of the critical surface tend to increase the divergence angle (Debayle *et al.*, 2010) and disrupt the structure of the fast electrons. Attosecond electron bunches generated during the interaction of an intense *p*-polarized laser pulse with solid targets have been observed and attributed to the pulling by the oscillating laser electric field (Naumova *et al.*, 2004; Ma *et al.*, 2006; Yang *et al.*, 2011). Such bunches can be generated in LWFA because of a strong chirp in the betatron frequency (Luttikhof *et al.*, 2010). In addition, a series of flying electron layers are generated during a 1.6 PW tightly focused laser pulse interacting with a thin foil target, which are suitable as relativistic mirrors for producing high intensity X-rays and γ-rays by reflecting counter propagating laser pulse (Bulanov *et al.*, 2010). Most existing studies on fast-electron generation are focused on the energy spectrum of the electrons and the efficiency of energy conversion from the laser to the latter. The spatial structure of the fast electrons is rarely investigated. Information on the spatial structure of the electrons can be useful in identifying their generation mechanisms and potential applications.

In this paper, we shall focus on the spatial distribution of the fast electrons generated during the interaction of an ultraintense laser pulse with a solid target that has a subcritical preplasma. The preplasma has an exponentially increasing density profile of scale length ~8 μm, corresponding to that created by a prepulse of intensity 10^{12} W/cm^2, duration 1 ns, and energy ~1 mJ (corresponding to the Vulcan laser system at the Rutherford Appleton Laboratory). Electrons are accelerated and heated as the laser pulse propagates in the preplasma. The temperature of the electrons increases as they propagate. For large L_p, the electron temperature can become much higher than the ponderomotive energy. The fast electrons penetrate through the thin solid target and appear in the target-rear vacuum region with a hemispherical distribution that is periodic at the laser wavelength. This phenomenon can be attributed to betatron resonance absorption and laser self-focusing in the preplasma and the $v \times B$ acceleration of the fast electrons in the intense self-generated field in the conical focusing region. The periodic electron layers can be considered as highly nonlinear plasma waves whose peak density is much larger than the background density (here nearly zero) and can exhibit characteristics quite different from their linear counterparts (Lu *et al.*, 2010; Wang *et al.*, 2011; 2013). They may also be useful as plasma grating for chirped pulse amplification of laser pulse (Sheng *et al.*, 2003) as well as moving mirrors for producing tunable ultrashort-ultraintense and other novel radiation (Ostrovskii *et al.*, 1975; Zhuo *et al.*, 2012; Wu *et al.*, 2012).

SIMULATION MODEL AND RESULTS

To study the generation of the hemispherical fast electron waves, the relativistic 2D3V particle-in-cell (PIC) code LAPINE (Xu *et al.*, 2002) is used to simulate the interaction of an ultraintense laser pulse with the target. A plasma slab with density $50n_c$ and thickness $5\lambda_0$ is preceded by a subcritical preplasma, where $n_c = 1.12 \times 10^{21}$ cm^{-3} is the critical density and $\lambda_0 = 1$ μm is the laser wavelength. The density of the latter increases exponentially from $0.02n_c$ to n_c with a scale length $L_p = 8$ μm. In order to preclude the effects of ion acceleration and heating (Pretzler *et al.*, 1998), the plasma is assumed to consist of electrons and Al ions with mass $27m_p$ and charge $10e$, where $m_p = 1836\ m_e$ is the proton mass. The initial temperature of both the electrons and ions is 1 KeV. The simulation box is $60\lambda_0 \times 30\lambda_0$ with 2400×1200 cells, and 49 electrons and 16 Al ions per cell. A 10^{20} W/cm^2 ($a_0 = 8.54$) *p*-polarized laser pulse is incident normally from the left. Both the spatial and temporal profiles of the laser pulse are Gaussian. The laser spot radius is $5\lambda_0$ and the pulse duration is $40T_0$ (FWHM), where T_0~3.3 fs is the laser period. The simulation time step is $0.009T_0$. Absorbing boundary conditions are used for the fields and particles at all boundaries.

Figure 1 shows the distributions of the electron density (a), kinetic energy density (b), kinetic energy density along the radial direction (c), and the electron energy spectrum (d). One can see that a plasma channel is formed in the preplasma and several nonlinear processes take place there, including self-focusing, hole-boring, as well as filamentation, all of which can affect the generation and propagation of the fast electrons. The electrons are accelerated by the laser pulse as it propagates in the preplasma. The energetic electrons then penetrate the solid-density slab and enter into the backside vacuum region, where they exhibit a periodic hemispherical distribution with ~$0.2n_c$ density peaks and laser wavelength spacings, as shown in Figure 1c, in which the electron kinetic energy density distribution along the radial direction in the upper half-space is presented. Sun *et al.* (1987) showed that a laser pulse propagating in underdense plasma with a frequency of ω_p experiences relativistic self-focusing if the laser power P exceeds the critical power $P_{cr} \approx 17(\omega_0/\omega_p)^2$ GW, where ω_0 is the laser frequency. For the average density (~$0.25n_c$) of the preplasma, we obtain $P_{cr} \sim 6.7 \times 10^{11}$ W ($I = 2.7 \times 10^{17}$ W/cm^2 for the 5 μm spot radius here), so that the self-focusing condition is satisfied. Figure 2 shows the Poynting vector along the laser propagation axis. It can be seen that the laser pulse is indeed self-focused in the preplasma, resulting in a tight focal spot (~2 μm) at the solid-slab front. The phase velocity of the wave fronts propagating through a focusing medium can be approximated as (Gibbon, 2005)

$$v_p(r) = c\left[1 - \frac{\omega_p^2}{\omega_0^2(1 + a^2(r)/2)^{1/2}}\right]^{-1/2} \sim c\left[1 + \frac{\omega_p^2}{2\omega_0^2}\left(1 - \frac{a^2(r)}{4}\right)\right],$$

https://doi.org/10.1017/S0263034613000359 Published online by Cambridge University Press

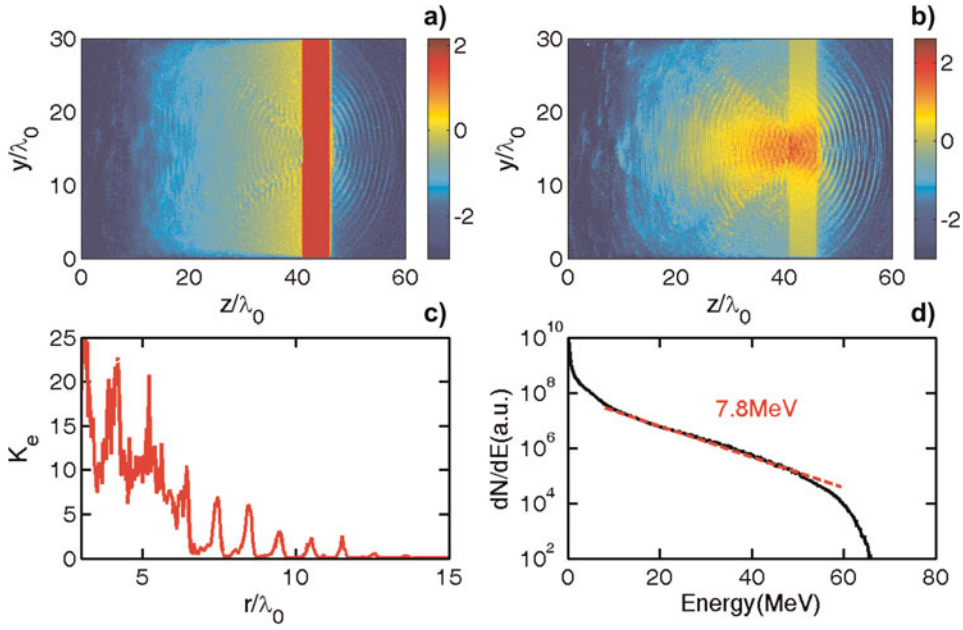

Fig. 1. (Color online) $\log_{10}$ of electron density (**a**) and electron kinetic energy density (**b**) distribution at $t = 90T_0$, respectively. The distribution of electron kinetic energy density along the radial direction at $t = 90T_0$ (**c**), whose origin of coordinate is at the midplane of the solid-slab front. The energy spectrum of the electrons at $t = 100T_0$ (**d**). The density is in units of n_c and the kinetic energy density is in units of $m_e c^2 n_c$ (same in the other figures).

where c is the light speed in vacuum and $a(r)$ is dimensionless radial profile of the laser. It shows that the phase fronts will propagate slower at the center than at the edge, thus inducing a curvature in the phase front and causing the light to bend. We can indeed see that self-focusing bends the laser wave fronts to a converging hemispherical profile. Figure 1b shows that the fast electron layers in the upper (lower) vacuum regions behind the target are generated in the lower (upper) regions of the preplasma. That is, the fast electrons from the preplasma cross the midplane as they propagate through the solid target layer. This is because the laser-light polarization in the preplasma is locally modulated by the self-focusing, leading to a $v \times B$ force on the electrons that drives them toward the midplane and beyond, while the electrostatic space-charge field arising from the laser expulsion of the preplasma electrons confines the latter's transverse excursion. The electron temperature can reach 7.8 MeV, with a cut-off energy at ~65 MeV, as can be seen in Figure 1d. The temperature T_h of fast electrons generated in intense laser-plasma interaction as given by the Wilks scaling law $T_h = m_e c^2(\sqrt{1 + a_0^2} - 1)$ (Wilks *et al.*, 1992) is $T_h = 3.9$ MeV (for $a_0 = 8.54$ as here), which is about half of that obtained in our simulation. Thus, the preplasma can enhance the acceleration of electrons. We also noted that the temperature distribution of the fast electrons behind the solid-slab is similar to that in Figure 1d except that the electron number is reduced slightly.

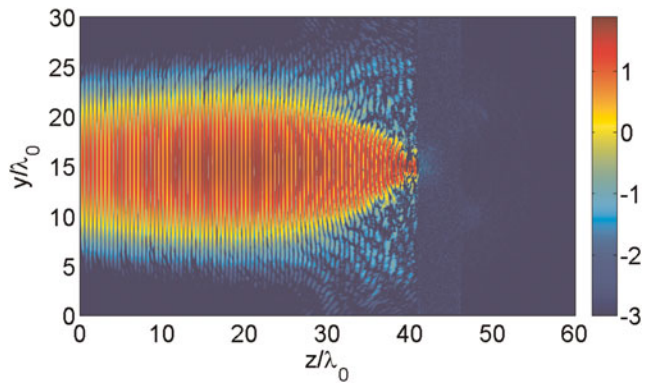

Fig. 2. (Color online) $\log_{10}$ of Poynting vector along the laser propagation axis $(\frac{c}{4\pi}(E \times B)_z)$ at $t = 70T_0$, only the positive energy flux is shown. The energy flux is in units of $m_e^2 c^3 \omega_0^3 / 4\pi e^2$.

Several mechanisms can produce high energy electrons in the underdense plasma. These include betatron resonance absorption, stochastic heating, and LWFA. In the present problem, the laser pulse duration is much larger than the plasma wavelength and the acceleration distance is very limited, so that the contribution of LWFA can be neglected. Stochastic heating can also be neglected. Figures 3a and 3b for the transverse and longitudinal electron phase space shows that the electrons oscillate in the laser electric field at the laser frequency. The transverse momentum of the electrons increases with the laser penetration distance and can reach a maximum of ~$70 m_e c$, which is about eight times higher than that (namely $P_y = a_0 m_e c = 8.5 m_e c$) of a relativistic electron in a plane electromagnetic wave in vacuum (Yu *et al.*, 2000). Since the electrons are also accelerated by the reflected

https://doi.org/10.1017/S0263034613000359 Published online by Cambridge University Press

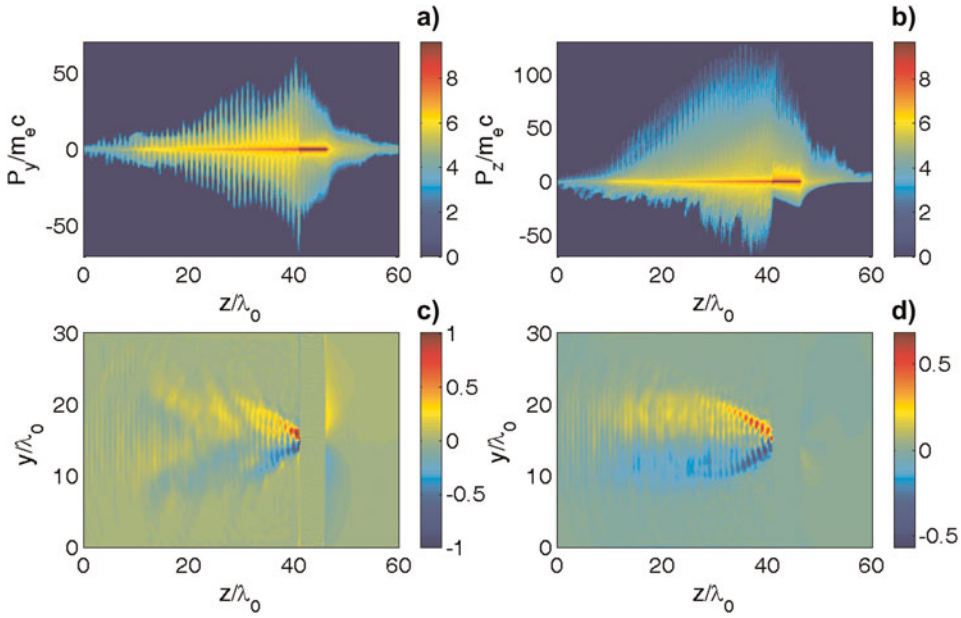

Fig. 3. (Color online) Distributions of the electron (**a**) transverse momentum (P_y) and (**b**) longitudinal momentum (P_z), and the (**c**) transverse quasistatic magnetic field (B_x), and (**d**) transverse electrostatic field (E_y) at $t = 80T_0$. The momentums are on $\log_{10}$ scale. The fields B_x and E_y have been averaged over eight laser periods and are in units of $m_ec\omega_0/e$.

laser pulse propagating backward in the preplasma, as indicated by the negative electron momentum ($P_z < 0$) near the slab target in Figure 3b, their transverse momentum is further increased. The transverse electron momentum in the wave is converted into longitudinal momentum by the $v \times B$ interaction, and P_z of the fast electrons can reach ~$110m_ec$, about three times that, namely $P_z = \frac{1}{2}a_0^2 m_ec = 36.5m_ec$ in vacuum (Yu *et al.*, 2000). As expected, we see that the oscillation frequency of the longitudinal momentum is twice that (ω_0) of the transverse momentum, accompanied by significant longitudinal heating (spread in the $z - P_z$ phase space).

The ponderomotive expulsion of electrons produces strong transverse charge-separation fields, as well as electron currents that generate quasistatic magnetic fields (Pukhov *et al.*, 1999), as can be seen in Figures 3c and 3d, where for clarity these fields have been averaged over eight laser periods. We can see that the quasistatic fields E_y and B_x remain periodic in space (whose spatial periods are comparable to the laser wavelength), and their maximum amplitudes occur at the boundaries of the self-focusing cone, where the electron density is also the highest. Accordingly, electrons are accelerated forward in layers into the opposite half-space behind the target by the v_yB_L force, where B_L is laser magnetic field and v_y is the speed of the electrons in the charge-separation field E_y. This also explains why the hemispherical electron layers have a slight phase mismatch at the midplane.

In order to see how the hemispherical electron waves are generated, we have also considered the interaction of a laser pulse with a solid density target without a preplasma, as well as with only a preplasma. Figure 4a shows that no hemispherical electron waves appear when there is only the solid-slab. As expected, only electron clouds appear at the front and back of the latter (Wilks *et al.*, 1992). On the other hand, Figure 4b shows that with only the preplasma, hemispherical waves are generated and propagate forward into the target backside region. That is, the preplasma is both necessary and sufficient for the generation of these waves. The temperature of the fast electrons can reach ~6.3 MeV, which is lower than that for the complete preplasma-solid layer system (Fig. 1). This can be attributed to the absence of laser pulse reflection, so that the recoil acceleration of electrons as well as additional heating by the reflected wave do not occur. In fact, most of the laser pulse penetrates through the target, with only a small amount of reflection from the conic regions where the density is snow-plowed to above-critical by the ponderomotive compression and self-focusing. From the frequency spectra of the self-generated electric fields for all the cases considered, we could not find evidence of stimulated Raman scattering (Gibbon, 2005). On the other hand, the energetic electrons oscillate periodically in both the transverse and longitudinal directions in the fields of the incident and reflected light waves, which means that the contribution of the stochastic heating by counter-propagating electromagnetic waves is insignificant in the situation. For completeness, Figures 4c and 4d show the electron kinetic energy density distributions for interactions of a circularly polarized (CP) and *s*-polarized (SP) laser pulse with the target plasmas. One can see that fast hemispherical electron waves with density peaks of ~$0.1n_c$ are generated by the CP pulse, and the crossed propagation of the hemispherical waves in the target, as discussed above. Although the $2\omega_0$ component from the $J \times B$ heating

https://doi.org/10.1017/S0263034613000359 Published online by Cambridge University Press

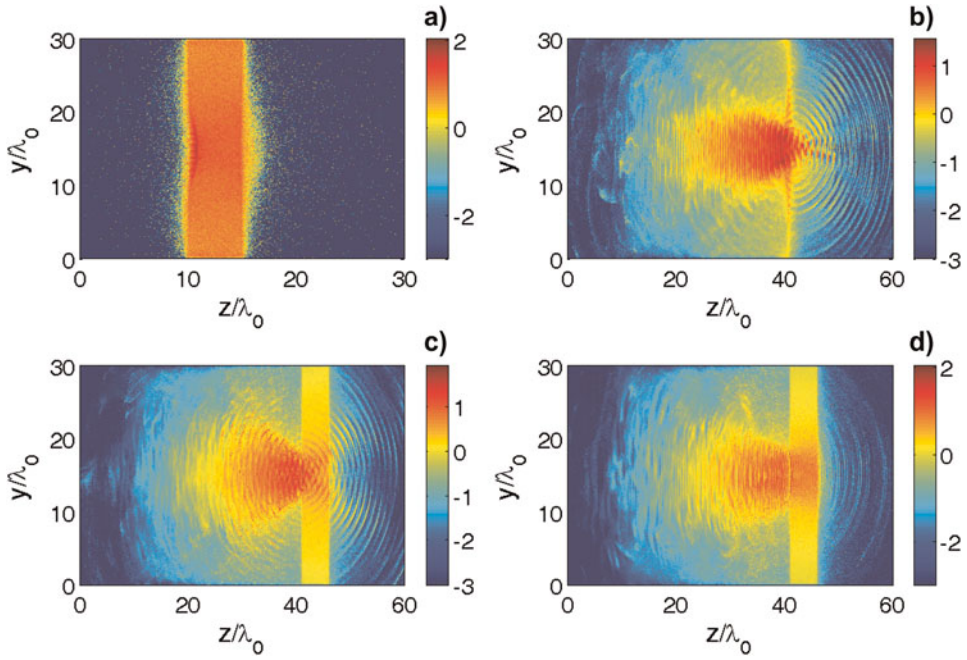

Fig. 4. (Color online) $\log_{10}$ of electron kinetic energy density distributions for the cases with a solid target without the preplasma (**a**), target of preplasma only (**b**), circularly polarized laser (**c**), and *s*-polarized laser (**d**) at $t = 90T_0$. The other parameters are the same as that in Figure 1.

(Kruer, 1985) is nearly absent, the electron temperature can still reach 5.2 MeV. However, hemispherical fast electron waves do not appear for the SP pulse. This can be attributed to the fact that here the laser electric field is not in the simulation plane. The electrons can still oscillate in the laser electric field, but the corresponding force of the quasistatic fields is missing in the electrons oscillating plane due to our 2D3V simulation. That is, the betatron resonance of the electrons does not occur.

For completeness, we also considered the effect of the scale length of the preplasma on the generation of hemispherical fast electron waves. One can see in Figure 5a that fast electron bunches with half wavelength spacing can be generated in a preplasma with $L_p = 2$ μm, but they do not have an obviously hemispherical profile. In addition, self-focusing of the laser pulse in the preplasma and the crossed propagation of the fast electron bunches in the target are not observed. In this regime, the $J \times B$ heating is still dominant, which leads to an electron temperature of 3.1 MeV, consistently with the Wilks' scaling (3.9 MeV). With increasing preplasma scale length, the hemispherical wave profile becomes more and more obvious. In fact, for $L_p = 12$ μm we still find fast hemispherical electron layers with ~$0.2n_c$ density peaks, as shown in Figure 5b, very similar to that for $L_p = 8$ μm. Because of limitation of our computation sources, we have not considered still longer scale lengths. However, it can be expected that hemispherical waves can still be generated as long as the laser pulse self focuses appropriately.

The effect of laser intensity on the generation of the hemispherical fast electron waves has also been investigated.

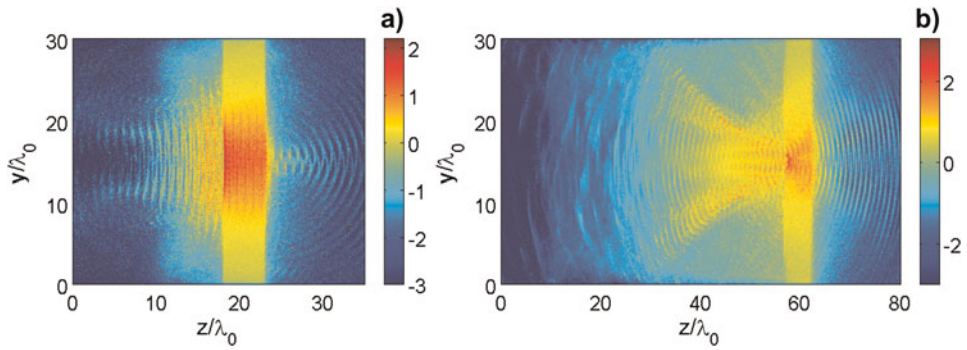

Fig. 5. (Color online) $\log_{10}$ of electron kinetic energy density distributions for the cases with scale length of preplasma 2 μm at $t = 70T_0$ (**a**) and 12 μm at $t = 120T_0$ (**b**), respectively. The laser intensity is fixed at 10^{20} W/cm^2.

https://doi.org/10.1017/S0263034613000359 Published online by Cambridge University Press

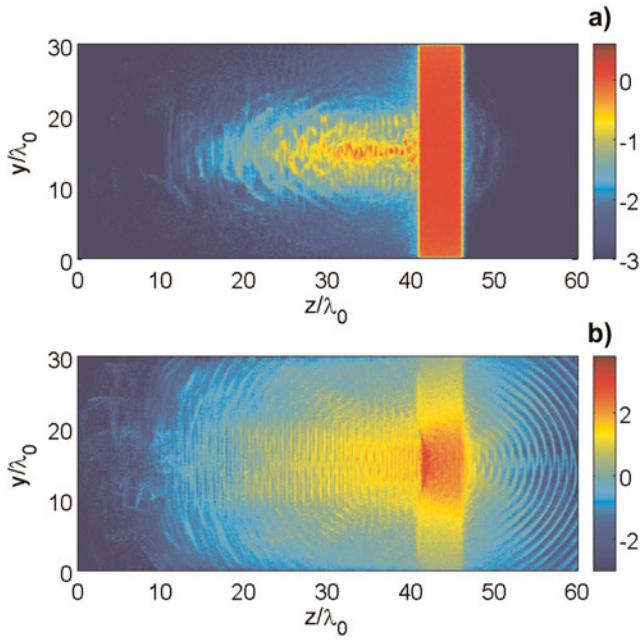

Fig. 6. (Color online) $\log_{10}$ of electron kinetic energy density distributions for the cases with laser intensity 10^{18} W/cm^2 (**a**) and 10^{21} W/cm^2 (**b**) at $t = 90T_0$, respectively. The scale length of the preplasma is fixed to 8 μm.

In Figure 6, we show the electron kinetic energy density distribution for the cases with laser intensity 10^{18} W/cm^2 and 10^{21} W/cm^2. It is found that the amplitude of the waves behind the target increases with the laser intensity. Furthermore, no waves are generated behind that target for $a = 10^{18}$ W/cm^2. This is consistent with the observation (Pukhov *et al.*, 1999) that for betatron resonance the laser power should significantly exceed (e.g., six times) the critical power for self-focusing.

In Figure 7a we show the dependence of the fast-electron temperature T_f on the preplasma scale length and the laser intensity. We see that the fast-electron temperature first increases rapidly with the preplasma scale length and then the increase slows down, although saturation was not found because of limitation in the size of our system. Figure 7b shows the dependence of the fast-electron temperature on the laser intensity for $L_p = 8$ μm. As expected, we have $T_f \sim 0.87a_0$, or $T_f \sim 0.74(I_{18}\lambda_{\mu m}^2)^{1/2}$, where I_{18} is the laser intensity in units of 10^{18} W/cm^2 and λ is the laser wavelength in units of μm. The fast-electron temperature obtained here is about half that in Pukhov *et al.* (1999), where a much longer preplasma ($L_p = 30$ μm) was used.

CONCLUSION

Intense laser interaction with matter in the presence of a subcritical preplasma having an exponentially increasing density profile (of scale length 2–12 μm) is studied using 2D3V PIC simulations for laser intensities 10^{18}–10^{21} W/cm^2. Hemispheric electron waves are generated at the back of the target if the laser intensity is sufficiently intense and the preplasma scale length sufficiently large (>5 μm). The electrons are efficiently accelerated by betatron resonance absorption as the intense laser pulse propagates and self-focuses in the preplasma. The temperature of the fast electrons increases with the preplasma scale length and can become much higher than that due to the ponderomotive acceleration. The fast electrons penetrate through the solid target and appear behind it as hemispheric distributed bunches at laser-wavelength spacings. The hemispheric waves can also be generated for CP lasers but not for SP lasers. The hemispheric waves can be useful as flying mirrors for producing bright ultra-short radiation in the KeV range (Bulanov *et al.*, 2012).

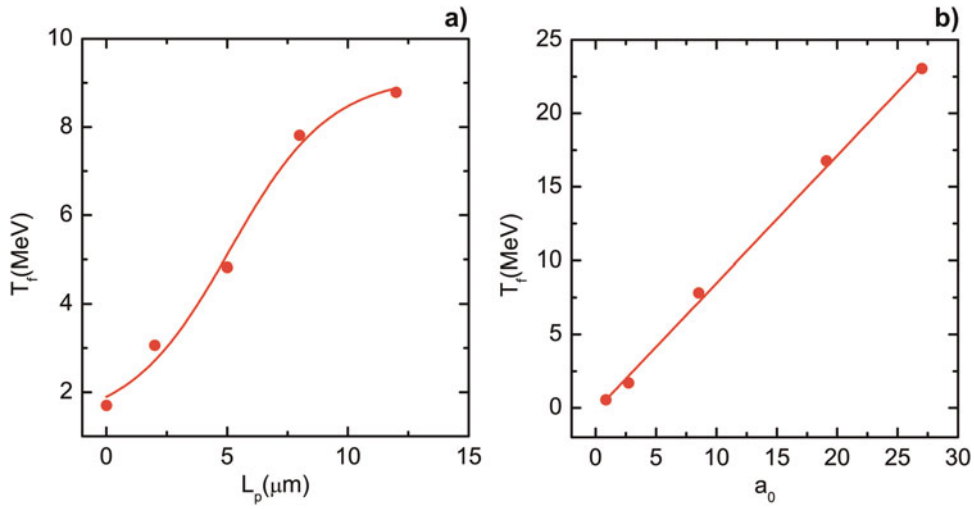

Fig. 7. (Color online) Fast electron temperature as a function of preplasma scale length (**a**) and dimensionless laser electric field (**b**), respectively. The laser intensity is fixed at 10^{20} W/cm^2 in (**a**), and the scale length of the preplasma is fixed to 8 μm in (**b**). The dots are PIC simulation results and the solid lines are the best fits of the latter.

https://doi.org/10.1017/S0263034613000359 Published online by Cambridge University Press

ACKNOWLEDGMENTS

This work was supported by NSFC (Grant Nos. 10975185, 10976031, 10835003, and 11275269) and SRFDP (Grant No. 20114307110020). M.B. acknowledges funding from projects ELI (Grant No. CZ.1.05/1.1.00/483/02.0061) and OPVK 3 (Grant No. CZ.1.07/2.3.00/20.0279). X.H.Y. also acknowledges the support from the China Scholarship Council, the Innovation Foundation for Postgraduate of Hunan Province (Grant No. CX2010B008) and NUDT (Grant No. B100204).

REFERENCES

Borghesi, M., Fuchs, J., Bulanov, S.V., Mackinnon, A.J., Patel, P.K. & Roth, M. (2006). Fast ion generation by high-intensity laser irradiation of solid targets and applications. *Fusion Sci. Technol.* **49**, 412–439.

Bulanov, S.S., Maksimchuk, A., Krushelnick, K., Popov, K.I., Bychenkov, V.Yu. & Rozmusc, W. (2010). Ensemble of ultrahigh intensity attosecond pulses from laserCplasma interaction. *Phys. Lett. A* **374**, 476.

Bulanov, S.S., Maksimchuk, A., Schroeder, C.B., Zhidkov, A.G., Esarey, E. & Leemans, W.P. (2012). Relativistic spherical plasma waves. *Phys. Plasmas* **19**, 020702.

Cai, H.B., Mima, K., Sunhara, A., Johzaki, T., Nagatomo, H., Zhu, S.P. & He, X.T. (2010). Prepulse effects on the generation of high energy electrons in fast ignition scheme. *Phys. Plasmas* **17**, 023106.

Davies, J.R. (2009). Laser absorption by overdense plasmas in the relativistic regime. *Plasma Phys. Control. Fusion* **51**, 014006.

Debayle, A., Honrubia, J.J., D'Humières, E. & Tikhonchuk, V.T. (2010). Characterization of laser-produced fast electron sources for fast ignition. *Plasma Phys. Control. Fusion* **52**, 124024.

Deutsch, C. & Didelez, J.P. (2011). Inertial confinement fusion fast ignition with ultra-relativistic electron beams. *Laser Part. Beams* **29**, 39–44.

Friou, A., Lefebvre, E. & Gremillet, L. (2012). Channeling dynamics of relativistic-intensity laser pulses. *Phys. Plasmas* **19**, 022704 (2012).

Gahn, C., Tsakiris, G.D., Pukhov, A., Meyer-ter-vehn, J., Pretzler, G., Thirolf, P., Habs, D. & Witte, K.J. (2000). Multi-MeV electron beam generation by direct laser acceleration in high-density plasma channels. *Phys. Rev. Lett.* **83**, 4772.

Gibbon, P. (2005). *Short Pulse Laser Interactions with Matter*. London: Imperial College Press.

Kemp, A.J., Cohen, B.I. & Divol, L. (2010). Integrated kinetic simulation of laser-plasma interactions, fast-electron generation, and transport in fast ignition. *Phys. Plasmas* **17**, 056702.

Kemp, A.J., Sentoku, Y. & Tabak, M. (2009). Hot-electron energy coupling in ultraintense laser-matter interaction. *Phys. Rev. E* **79**, 066406.

Kruer, W.L. (1985). $J \times B$ heating by very intense laser light. *Phys. Fluids* **28**, 430.

Lin, X.X., Li, Y.T., Liu, B.C., Liu, F., Du, F., Wang, S.J., Chen, L.M., Zhang, L., Liu, X., Liu, X.L., Wang, Z.H., Ma, J.L., Lu, X., Dong, Q.L., Wang, W.M., Sheng, Z.M.,, Wei, Z.Y. & Zhang, J. (2012). Directional transport of fast electrons at the front target surface irradiated by intense femtosecond laser pulses with preformed plasma. *Laser Part. Beams* **30**, 39–43.

Lu, G.M., Liu, Y., Zheng, S., Wang, Y.M., Yu, W. & Yu, M.Y. (2010). Exact relativistic plasma waves in an electron-positron plasma. *Astrophys. Space Sci.* **330**, 73.

Luttikhof, M.J.H., Khachatryan, A.G., Van goor, F.A. & Boller, K.J. (2010). Generating ultrarelativistic attosecond electron bunches with laser wakefield accelerators. *Phys. Rev. Lett.* **105**, 124801.

Ma, T., Sawada, H., Patel, P.K., Chen, C.D., Divol, L., Higginson, D.P., Kemp, A.J., Key, M.H., Larson, D.J., Le pape, S., Link, A., Macphee, A.G., Mclean, H.S., Ping, Y., Stephens, R.B., Wilks, S.C. & Beg, F.N. (2012). Hot electron temperature and coupling efficiency scaling with prepulse for cone-guided fast ignition. *Phys. Rev. Lett.* **108**, 115004.

Ma, Y.Y., Sheng, Z.M., Li, Y.T., Chang, W.W., Yuan, X.H., Chen, M., Wu, H.C., Zheng, J. & Zhang, J. (2006). Dense quasi-monoenergetic attosecond electron bunches from laser interaction with wire and slice targets. *Phys. Plasmas* **13**, 110702.

Macphee, A.G., Divol, L., Kemp, A.J., Akli, K.U., Beg, F.N., Chen, C.D., Chen, H., Hey, D.S., Fedosejevs, R.J., Freeman, R.R., Henisian, M., Key, M.H., Le pape, S., Link, A., Ma, T., Mackinnon, A.J., Ovchinnikov, V.M., Patel, P.K., Phillips, T.W., Stephens, R.B., Tabak, M., Town, R., Tsui, Y.Y., Van woerkom, L.D., Wei, M.S. & Wilks, S.C. (2010). Limitation on prepulse level for cone-guided fast-ignition inertial confinement fusion. *Phys. Rev. Lett.* **104**, 055002.

Nilson, P.M., Solodov, A.A., Myatt, J.F., Theobald, W., Jaanimagi, P.A., Gao, L., Stoeckl, C., Craxton, R.S., Delettrez, J.A., Yaakobi, B., Zuegel, J.D., Kreschwitz, B.E., Dorrer, C., Kelly, J.H., Akli, K.U., Patel, P.K., Mackinnon, A.J., Betti, R., Sangster, T.C. & Meyerhofer, D.D. (2011). Scaling hot-electron generation to long-pulse, high-intensity laser-solid interactions. *Phys. Plasmas* **18**, 056703 (2011).

Naumova, N., Sokolov, I., Nees, J., Maksimchuk, A., Yanovsky, V. & Mourou, G. (2004). Attosecond electron bunches. *Phys. Rev. Lett.* **93**, 195003.

Nuter, R., Gremillet, L., Combis, P., Drouin, M., Lefebvre, E., Flacco, A. & Malka, V. (2008). Influence of a preplasma on electron heating and proton acceleration in ultraintense laser-foil interaction. *J. Appl. Phys.* **104**, 103307.

Ostrovskii, L.A. (1975). Some "moving boundaries paradoxes" in electrodynamics. *Sov. Phys. Usp.* **18**, 452.

Paradkar, B.S., Wei, M.S., Yabuuchi, T., Stephens, R.B., Larsen, J.T. & Beg, F.N. (2010). Numerical modeling of fast electron generation in the presence of preformed plasma in laser-matter interaction at relativistic intensities. *Phys. Rev. E* **83**, 046401.

Pfeifer, T., Spielmann, C. & Gerber, G. (2006). Femtosecond x-ray science. *Rep. Prog. Phys.* **69**, 443.

Pretzler, G., Saemann, A., Pukhov, A., Rudolph, D., Schätz, T., Schramm, U., Thirolf, P., Habs, D., Eidmann, K., Tsakiris, G.D., Meyer-ter-vehn, J. & Witte, K.J. (1998). Neutron production by 200 mJ ultrashort laser pulses. *Phys. Rev. E* **58**, 1165.

Pukhov, A. & Meyer-ter-vehn, J. (1996). Relativistic magnetic self-channeling of light in near-critical plasma: three-dimensional particle-in-cell simulation. *Phys. Rev. Lett.* **76**, 3975.

Pukhov, A., Sheng, Z.M. & Meyer-ter-vehn, J. (1999). Particle acceleration in relativistic laser channels. *Phys. Plasmas* **6**, 2847.

Sakagami, H., Sunahara, A., Johzaki, T. & Nagatomo, H. (2012). Effects of long rarefied plasma on fast electron generation for FIREX-I targets. *Laser Part. Beams* **30**, 103–109.

Sentoku, Y., Kruer, W., Matsuokal, M. & Pukhov, A. (2006). Laser hole boring and hot electron generation in the fast ignition scheme. *Fusion Sci. Technol.* **49**, 278–296.

Sheng, Z.M., Mima, K., Sentoku, Y., Jovanovi, M.S., Tauguchi, T., Zhang, J. & Meyer-ter-vehn, J. (2002). Stochastic heating and acceleration of electrons in colliding laser fields in plasma. *Phys. Rev. Lett.* **88**, 055004.

Sheng, Z.M., Zhang, J. & Umstadter, D. (2003). Plasma density gratings induced by intersecting laser pulses in underdense plasmas. *Appl. Phys. B* **77**, 673.

Sun, G.Z., Ott, E., Lee, Y.C. & Guzdar, P. (1987). Self-focusing of short intense pulses in plasmas. *Phys. Fluids* **30**, 526.

Tajima, T. & Dawson, J.M. (1979). Laser electron accelerator. *Phys. Rev. Lett.* **43**, 267.

Tabak, M., Hammer, J., Glinsky, M.E., Kruer, W.L., Wilks, S.C., Woodworth, J., Campbell, E.M., Perry, M.D. & Mason, R.J. (1994). Ignition and high gain with ultrapowerful lasers. *Phys. Plasmas* **1**, 1626.

Wang, Y.M., Yu, M.Y. & Chen, Z.Y. (2011). Coherent relativistic wake wave of a charged object moving steadily in a plasma. *Phys. Scr.* **31**, 155.

Wang, Y.M., Yu, M.Y., CHEN, Z.Y. & Lu, G.M. (2013). Excitation of large amplitude wake electron oscillations in adiabatic plasma. *Laser Part. Beams* **84**, 025501.

Wei, M.S., Solodov, A.A., Pasley, J., Stephens, R.B., Welch, D.R. & Beg, F.N. (2008). Study of relativistic electron beam production and transport in high-intensity laser interaction with a wire target by integrated LSP modeling. *Phys. Plasmas* **15**, 083101.

Wilks, S.C., Kruer, W.L., Tabak, M. & Langdon, A.B. (1992). Absorption of ultra-intense laser pulses. *Phys. Rev. Lett.* **69**, 1383.

Wu, H.C. & Meyer-ter-vehn, J. (2012). Giant half-cycle attosecond pulses. *Nature Photonics* **6**, 304.

Xu, H., Chang, W.W. & Zhuo, H.B. (2002). Parallel programming of 2D3V PIC under distributed-memory parallel enviroments. *Chin. J. Comput. Phys.* **19**, 305 (in Chinese).

Yang, X.H., Ma, Y.Y., Shao, F.Q., Xu, H., Yu, M.Y., Gu, Y.Q., Yu, T.P., Yin, Y., Tian, C.L. & Kawata, S. (2010). Collimated proton beam generation from ultraintense laser-irradiated hole target. *Laser Part. Beams* **28**, 319–325.

Yang, X.H., Xu, H., Ma, Y.Y., Shao, F.Q., Yin, Y., Zhuo, H.B., Yu, M.Y. & Tian, C.L. (2011). Propagation of attosecond electron bunches along the cone-and-channel target. *Phys. Plasmas* **18**, 023109.

Yu, W., Bychenkov, V., Sentoku, Y., Yu, M.Y., Sheng, Z.M. & Mima, K. (2000). Electron acceleration by a short relativistic laser pulse at the front of solid targets. *Phys. Rev. Lett.* **85**, 570.

Yu, T.P., Chen, M. & Pukhov, A. (2009). High quality GeV proton beams from a density-modulated foil target. *Laser Part. Beams* **27**, 611–617.

Zhuo, H.B., Jin, Z., Yu, M.Y., Sheng, Z.M., Xu, H., Ma, Y.Y., Yin, Y., Shao, F.Q., Zhou, W.M. & Kodama, R. (2012). Strong mid-infrared radiation from self-guided fast electron bunch propagating along a grated target surface in laser-solid interaction. *Phys. Plasmas* **19**, 043108.